PERIODICA POLYTECHNICA SER. MECH. ENG. VOL. 50, NO. 1, PP. 27–36 (2006)

FINITE ELEMENT CONTACT AND THERMAL PREDICTION OF SURFACE FAILURE DURING DRY FRICTION OF A STEEL-ALUMINA SLIDING PAIR

Zoltán LESTYÁN, Károly VÁRADI and Albert ALBERS

Institute of Machine Design,
Budapest University of Technology and Economics,
Budapest, Műegyetem rkp. 3., H-1111, Hungary,
Email: lestyan.zoltan@gszi.bme.hu, varadik@eik.bme.hu, Url.: http://www.gszi.bme.hu,
Phone: +36 1 463 3509, Fax.: +36 1 463 3505
Institute of Product Development Karlsruhe,
University of Karlsruhe,
Karlsruhe, Kaiserstraße 10., D-76131, Germany,
Email: albers@ipek.uni-karlsruhe.de, Url.: http://www.ipek.uni-karlsruhe.de,
Phone: +49 (721) 608-2371, Fax.: +49 (721) 608- 6051

Received: April 11, 2006

Abstract

Contact and thermal pulsating and oscillating stresses can play an important role in surface failure. This study models the physical processes occurring in the contact area by contact and thermal simulations as well as present experimental results. The real contact area was determined on the basis of the surface topographies of worn sliding pairs, then the temperature developed in the contact area was simulated. When evaluating data, contact and thermal processes were analysed producing pulsating and oscillating stresses generated by the moving contact area passing through the sliding contact. The results justify the analysis and provide a basis for further research steps.

Keywords: dry friction, real contact, contact and thermal analysis, surface failure.

1. Introduction

The good heat conduction properties, high compression strength, wear resistance, the thermal and chemical stability, and the electric insulation ability of alumina ceramics make it a promising friction material for drive systems and brakes. As alumina ceramics is rigid, it is expedient to be coupled with a tough, elastic material with good heat conduction properties, such as steel. Applications extend to a number of power transmission systems. However, many questions need to be answered, with particular regard to surface failure processes, the knowledge of which is essential from the viewpoint of reliable operation. The joint impact of many phenomena determines surface failure processes, which are as follows:

- Real surface topographies produce discrete real contact areas in the course of sliding friction. Their extension has been studied, among others, by VÁRADI

et. al [11]. Considerable local contact pressure is generated along the contact areas consisting of point-like discrete areas, which can frequently cause elastic-plastic deformations.

- Increasing strain rate in the case of crystalline materials increases the yield point (GILLEMOT [4]), which is closely related to increased dislocation density.
- High temperature leads to reduce the yield point and therefore it also induces high degrees of plastic deformation. Heat expansion by temperature rise defines new geometrical boundary conditions for contact. TIAN and KENNEDY [8] developed an experimental test to determine the high temperatures generated in the contact area, while ARSLAN [1], TKACHUK [9], and VERNERSSON [12] used high-speed thermo-graphic camera recordings to determine temperature distribution in the vicinity of the contact area. There are a number of analytic (BOS and MOES [2]) and numerical (VÁRADI [10]) studies on heat generation in the contact area.
- Temperature-dependent mechanical and thermal material properties have a considerable impact on changes of the real contact area and heat generation. LING and RICE [7] examined the impact of temperature-dependent thermal material properties on thermal processes; HOU and KOMANDURI [5] demonstrated their impact on contact temperature in the course of the thermal examination of grinding.
- Material tests from new aspects are required by the great extent of deformation, the material composition of the near surface layer different from the basic material as well as its structure and mechanical behaviour. ELEÖD [3] analyses the non-linear material behaviour of the near surface layer, presenting the processes in the crystal structure.

The coupled modelling of the phenomena above makes it possible to properly describe actual processes and familiarize more with failure processes. Most of the phenomena above cannot be fully modelled together as yet, but approximative model calculations may provide a basis for further studies.

Our study is intended to investigate the contact and temperature processes caused by the contact area passing through the surface of the stationary steel disc. The real contact area and pressure distribution as well as the resulting heat generation change in time and space in the course of sliding. Changes may be highly intensive; in the case of temperature peaks, KENNEDY [6] reports on temperature flashes of 1000 °C of 10 ms duration.

The following assumptions were used in the course of our studies:

- The distribution of the contact area in space and time is independent from heat generation.
- A linear elastic material model was applied.
- Material properties at room temperature were considered.

The first step is to determine the real contact area and then to perform the thermal simulation of dry friction. The second step is the study and analysis of pulsating contact and thermal surface stresses.

2. The Friction Test and the Measured Microtopography

Physical and mechanical processes during dry friction were analysed by friction tests. The test rig is shown in *Fig. 1*. The friction test consisted of 300 test cycles. In the course of the test, 6 high-test ceramic palettes fixed in the revolver head on the same pitch circle were pushed against the stationary steel disc, then the palettes were rotated by constant angular acceleration. *Fig. 2* shows the changes of the number of revolutions and of the pressing force in the course of one cycle. During the steps of the experiment, rotational speed and the friction torque were measured. The pressing force was a constant 100N of each ceramic; the friction torque decreased in the course of sliding. The data measured provide a basis for subsequent contact and thermal calculations.

The temperature of the contact area of the sliding ceramic was measured by a high-speed thermo-graphic camera after each revolution, through a hole drilled into the steel disc (*Fig. 1*). The measured average and the maximum temperature were to verify the thermal simulation.

A Perthen stylus instrument was used for measuring 3D surface roughness in order to determine the topography of the worn sliding pairs after 300 test cycles. The sampling resolution of the surface roughness measurement was 50 μm. Worn surface topographies are shown in *Figs. 3* and *4*; plato-type wear was produced on the ceramic palette and a wear groove on the surface of the steel disc.

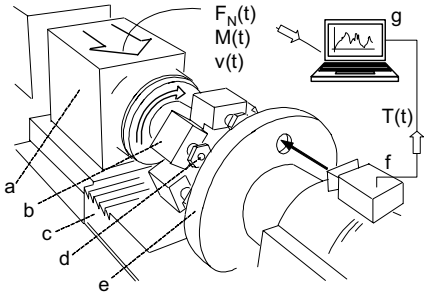

Fig. 1. The assembly of the test rig: the power train (a), rotating gripping head (b), feeding unit (c), ceramic palettes (d), stationary steel disc (e), thermo-graphic camera (f) and computer (g).

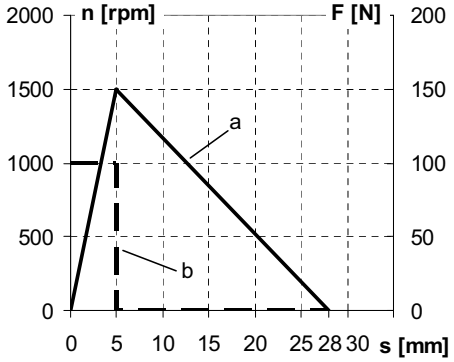

Fig. 2. The speed (a) and the pressing force per ceramic palette (b) in time in the course of one cycle.

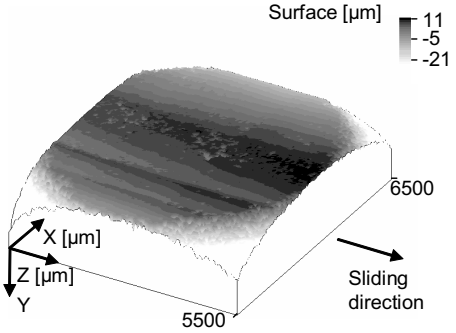

Fig. 3. The surface roughness of the table like worn surface of a ceramic palette after 300 repetitions.

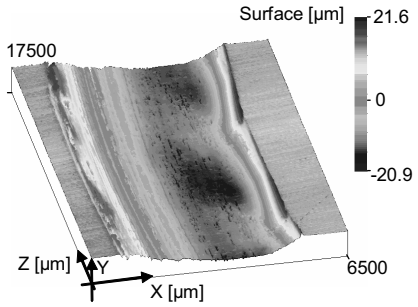

Fig. 4. The surface roughness of the worn groove of the steel disc after 300 repetitions.

3. FE Contact Model

The purpose of the FE contact calculation was to simulate the actual contact behaviour of the 0.5 mm long sliding. The contact calculation is determined by the topographies of actual worn surfaces. The topographies were used for defining the spatial distribution of the initial gap between the sliding pairs, which is the initial condition for the contact calculation. The FE mesh contains the ceramic and steel contact components. The area analysed is 5.5 mm per 6.5 mm, covering the entire contact area. The FE mesh contained 481289 nodes, 344297 elements, and 466 contact elements. The smallest unit of the mesh – the size of a single element on the contact surface of the model – was 50 μm by 50 μm. The load of the model was surface pressure corresponding to 100 N of pressing force, with boundary conditions as rigid supports, see *Fig. 5*. In the course of the contact simulation, a sliding simulation based on an incremental technique was performed in 10 steps. The step interval was 50 μm which was the smallest unit of surface roughness measurements and of the FE mesh.

Based on the contact calculation, many spot contacts were generated; therefore a square surface of 50 μm by 50 μm was defined in each point of contact, which corresponds to the FE discretization of the model. On this basis, the actual contact area was established in each step. Subsurface stress states were determined by substitute FE stress calculations based on the definition of the contact area above. The substitute model was subjected to surface pressure in step j and at location i, the direction of which encloses a semi-cone-angle of friction with the surface normal and its magnitude was defined as follows:

$$p_{i,j} = \sqrt{\left(p_{Ni,j}\right)^2 \left(1 + \mu_j^2\right)}, \tag{1}$$

$$p_{N_{i,j}} = F_{ci,j}/A^*, \tag{2}$$

where

$p_{i,j}$	is the applied pressure,
$p_{Ni,j}$	is the normal surface pressure,
$F_{ci,j}$	is the contact force at location i and in step j;
μ_j	is the coefficient of friction in step j,
A^*	is the discreet contact surface of a constant size of 50 μm per 50 μm.

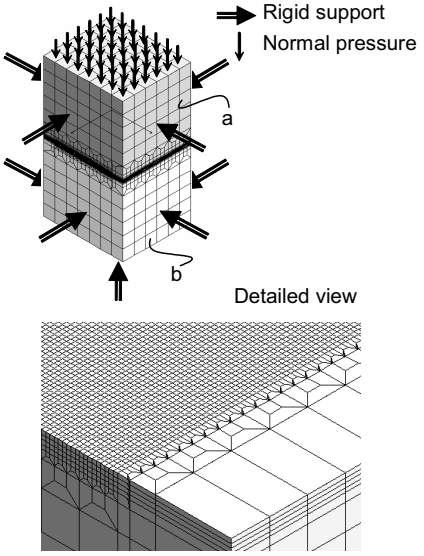

Fig. 5. The contact FE model, load, boundary conditions and material discretization: (a) ceramic, (b) steel. The detailed view of the steel side mesh.

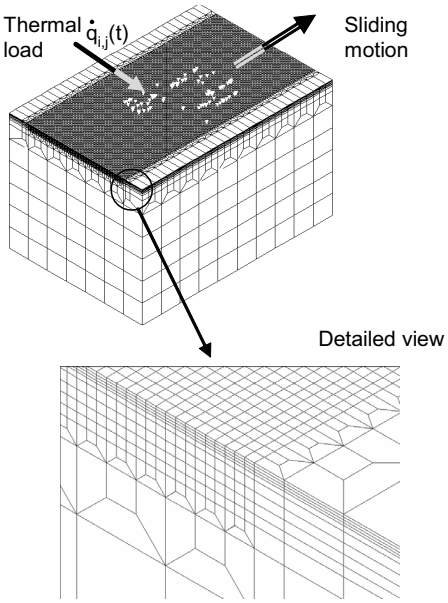

Fig. 6. The transient thermal model of steel surface: mesh, load, detailed view of mesh.

4. Transient FE Thermal Model

The thermal simulation of dry friction can be used for coming to know the temperature state generated during the first 1/6 revolution of the experimental test, corresponding to 88.5 mm sliding distance. The temperature simulation was based on a series of solutions to represents the moving heat sources, its step intervals corresponded to those of the contact simulation, that was 50 μm. As the boundary

conditions of thermal sliding simulation include the calculated (momentary) actual contact area and pressure distribution, the results of the 0.5 mm contact sliding were repeated 177 times.

In the course of FE transient thermal analysis, the thermal models of the ceramic and the steel were prepared. The magnitude and distribution of the thermal load of the ceramic side changed in space according to the real contact area and pressure distribution pertaining to the current step, while the heat source did not move in the direction of sliding. On the other hand, the distribution and magnitude of the thermal load of the steel side changed in each step according to the real contact area and pressure distribution pertaining to the current step, while the heat source was moving with constant acceleration along the steel surface. The two models were 'linked' by the heat partition affecting the distribution of heat generation, determined previously by an iterative algorithm and FE models. The FE mesh consisted of 347,317 elements in case of the ceramic and of 425,173 elements in case of the steel model (*Fig. 6*); the smallest unit of the mesh – the size of a single element on the contact surface – was 50 μm. In case of the ceramic, the area studied was 6.5 mm per 5.55 mm, while in the case of the steel it was 6.5 mm per 88.5 mm. The thermal load of the models was heat flux $q^{\cdot}_{i,j}$, which can be interpreted as follows at location i and in step j:

$$q^{\bullet}_{i,j} = p_{N_{i,j}} \mu_j v_j \beta_j \quad \text{in the case of steel side,} \tag{3}$$

$$q^{\bullet}_{i,j} = p_{N_{i,j}} \mu_j v_j (1 - \beta_j) \quad \text{in the case of ceramic side,} \tag{4}$$

where

v_j is the sliding velocity and

ß$_j$ is the heat partition of the steel side in step j.

In the course of thermal simulation, changes in the velocity and the friction coefficient are shown in *Fig.7*, and changes in the heat partition are shown in *Fig.8*. Surface heat transfer was negligible in the contact area and its immediate environment.

5. Results

Fig. 9 shows the surface pressure results at step 10 of the contact simulation. It can be observed that the surface pressure changes considerably in the contact area. Surface pressure values reach 930 MPa, while they are around 500 MPa on average. *Fig. 10* shows the von Mises equivalent stress distribution on the steel surface in the area of the point subjected to the highest stress. The von Mises equivalent stress reaches the highest value in the 12.5 μm range below the surface. For the purposes of later investigations, this point is indicated as point A on the steel surface.

Two evaluations are performed: one of them involves the study of contact and thermal phenomena in a relative coordinate system fixed to the moving ceramic palette. In the other one, the steel disk is analysed from a coordinate system assigned

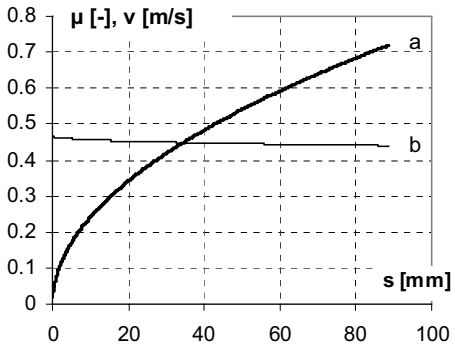

Fig. 7. The sliding velocity (a), the coefficient of friction (b), in the function of sliding distance.

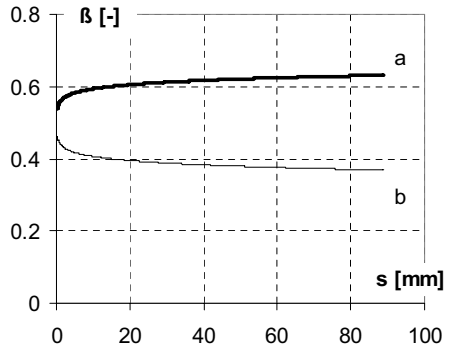

Fig. 8. The heat partition in sliding distance, in case of the steel side (a), in the case of the ceramic side (b).

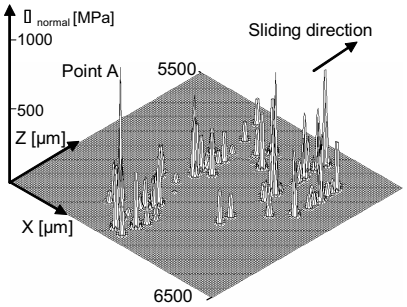

Fig. 9. The contact pressure distribution of the simulation for the steel surface at step 10.

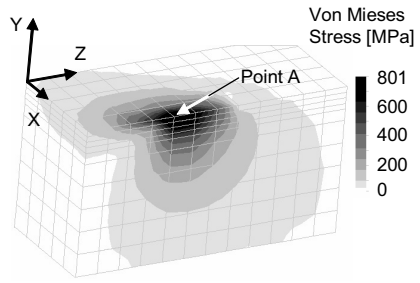

Fig. 10. The Mises stress distribution in the local environment of point A.

to a geometrical point of the steel surface how the ceramic passes through the point selected (point A).

The first type of test is used for studying the change of maximum temperature in the course of the sliding simulation, then the calculations are compared with the measurement results. *Fig. 11* shows the changes in the maximum temperatures of the sliding pairs in the function of sliding distance. The deviation of maximum contact temperatures is below 7 %. The maximum temperature reaches 210 °C during the 1/6 revolution, occurring in 0.246 s. *Fig. 12* shows a comparison between the maximum contact temperature of the ceramic palletes and the results of temperature measurements by a thermo-graphic camera. Calculation results show good agreement with temperature results. The comprehensive verification of the

numerical results of the warming up process requires highly calculation-intensive simulation later on.

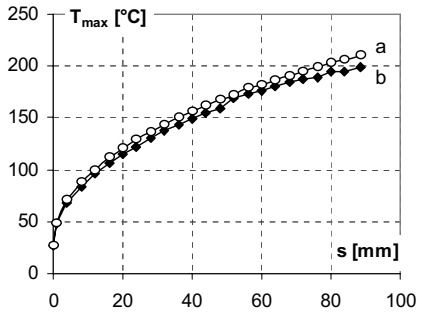

Fig. 11. The maximum temperatures calculated for the steel side (a) and ceramic side (b) in function of the sliding distance.

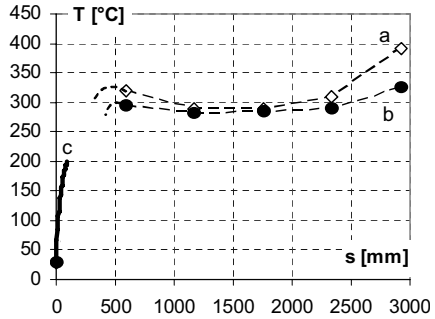

Fig. 12. The temperature results of calculation and measurement: the measured maximum (a) and mean (b) temperatures; calculated maximum temperature of ceramic side (c).

The second type of test involves the examination of the impact of the momentary contact areas passing through point A on the steel surface. The contact area passes through this point in 8 ms, while the ceramic covers a sliding distance of 84 mm to 90 mm. The momentary contact areas passing through point A cause pulsating stress in point A; *Fig. 13* shows the von Mises equivalent stress in time. A number of stress peaks are generated; some of them are over 800 MPa. *Fig. 13* shows the von Mises equivalent stress gradient in time, reflecting the intensity of pulsating stress. Changes of the Von Mises equivalent stress reach 10000 MPa/ms; in the majority of cases it is below the value of 4000 MPa/ms.

Similar phenomena can be observed in the change of temperature conditions: the temperature changes highly intensively (*Fig. 15*), causing temperature peaks of various sizes. The speed of temperature change goes up to as much as 1000 °C/ms (*Fig. 16*). In the layer close to the surface, the phenomena above can greatly contribute to surface failure. The speed of change depends on the velocity of sliding. Contact and thermal pulsating phenomena are highly intensive, although the sliding velocity is only 0.72 m/s at this moment. On the contrary, at the 5th second of our experiment, the sliding velocity reaches the value of 14.6 m/s. The pulsating phenomena generated probably play a major role in surface failure. Further statements thereon, however, can only be made in the accurate knowledge of the behaviour of materials.

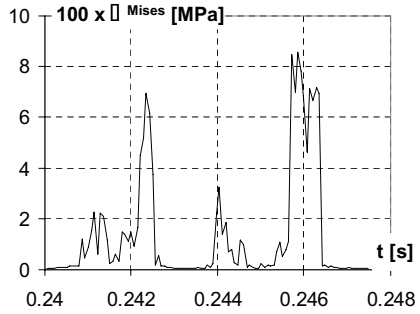

Fig. 13. The von Mises stress in time while the contact area is sliding above point A.

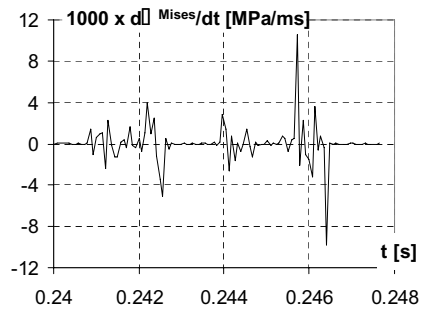

Fig. 14. The von Mises equivalent stress gradient in time while the contact area is sliding above point A.

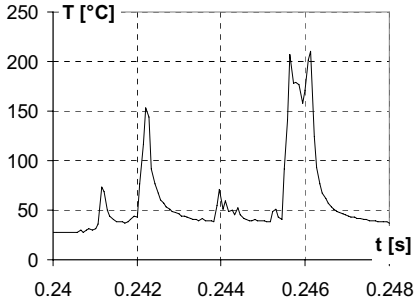

Fig. 15. The contact temperature in time while the contact area is sliding above point A.

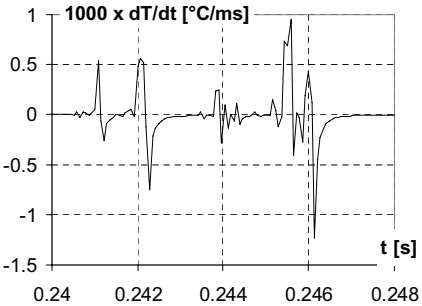

Fig. 16. The contact temperature gradient in time while the contact area is sliding above point A.

6. Conclusions

The FE contact and transient thermal algorithms can describe the real contact behaviour and the thermal processes. The contact behaviour shows local ”events”, producing high stresses. The portion of the real contact area is changing between 1.2 % and 1.5 % of the nominal contact area. The total generated heat can be transferred through small discrete areas thus high contact temperature values occur in a very short time.

The equivalent stresses and temperature distribution below the surface is concentrated in the upper 12.5 micron region. The contact area moving through the surface of the steel disk generates highly intensive stress and temperature fluctuations during the 8 ms period of passing. Numerous stress and temperature impulses

are generated while the contact area passes through. The von Mises equivalent stress in time reaches the value of 10,000 MPa/ms, while the temperature change in time is 1000-1200 °C/ms. Large fluctuations may play a considerable role in surface failure.

A local micro model is needed in the near future, to analyse the elastic-plastic contact and transient thermal behaviour of the asperities in a longer period of the sliding movement.

Acknowledgement

The authors would like to express their thanks to the Hungarian-German Partnership Project (MÖB-DAAD) for the financial support of mobility.

References

[1] ARSLAN, A. – ALBERS, A., Potenzialabschätzung von Belängen aus monolithischer Keramik in Trockenlaufenden Friktionssystemen und die Auswirkungen auf die Systemkonstruktion, 2. Satuskolloquium des SFB 483, 2004, Karlsruhe, Germany (Editor: K.-H. Zum Gahr), ISBN 3-933733-04-9, pp. 5–12.

[2] BOS, J. – MOES, H., Frictional Heating of Tribological Contacts, *Journal of Triblogy Transactions of ASME,* **117** (1995), pp. 171–177.

[3] ELEÖD, A., Deformation induced transient and stationary changes of the near-surface layer, Proceedings of Viennano 05', 2005, Vienna, Austria (Editors: W. J. Bartz and F. Franek), ÖTG, ISBN 3-901657-17-7, pp. 149–157.

[4] GILLEMET, L., *Anyagszerkezettan és anyagvizsgálat*, Tankönyvkiadó, Budapest, 1972

[5] HOU, Z. B. – KOMANDURI, R., On the Mechanics of the Grinding Process, Part II-Thermal analysis of fine grinding, *Int. Journal of Machine Tools & Manufacture,* **44** (2004), pp. 247–270.

[6] KENNEDY, F. E., Determination of contact temperatures resulting from frctional heating, *Proceedings of the International Tribology Conference, 2000, Nagasaki*, Japan, pp. 313–318.

[7] LING, F. F. – RICE, J. C., Surface Temperatures with Temperature-dependent Thermal Properties, *ASME Transactions,* **9** (1966), pp. 195–201.

[8] TIAN, X. – KENNEDY, F. E. – DEACUTIS, J. J. – HENNING, A. K., The Development and Use of thin Film Thermocouples for Contact Temperature Measurement, *Journal of Triblogy Transactions of ASME,* **35** (1992), pp. 491–499.

[9] TKACHUK, D. V. – BOGDANOVICH, P. N., Thermal Processes at High Speed Friction, *International Journal of Applied Mechanics and Engineering Special issue ITC 2004,* **9** (2004), pp. 177–182.

[10] VÁRADI, K. – NÉDER, Z. – FRIEDRICH, K. – FLÖCK, J., Numerical and Finite Element Contact Temperature Analysis of Real Composite-steel Surfaces in Sliding Contact, *Tribology international,* **31** (1999), pp. 669–686.

[11] VÁRADI, K. – NÉDER, Z. – FRIEDRICH, K. – FLÖCK, J., The Real Contact Area between Composite and Steel Surfaces in Sliding Contact, *Composites Science and Techology,* **61** (2001), pp. 1853–1862.

[12] VERNERSSON, T., Thermally Induced Roughness of Tread-braked Railway Wheels Part 1: Brake Rig Experiments, *Wear,* **236** (1999), pp. 96–105.